

MBE Growth and Characterization of Strained HgTe (111) Films on CdTe/GaAs *

Jian Zhang(张健)^{1,2}, Shengxi Zhang(张圣熙)^{1,2}, Xiaofang Qiu(邱小芳)¹, Yan Wu(巫艳)^{1**}, Qiang Sun(孙强)³, Jin Zou(邹进)^{3,4}, Tianxin Li(李天信)^{1,2}, Pingping Chen(陈平平)^{1,2**}

¹State Key Laboratory of Infrared Physics, Shanghai Institute of Technical Physics, Chinese Academy of Sciences, Shanghai 200083

²University of Chinese Academy of Sciences, Beijing 100049

³Materials Engineering, The University of Queensland, Brisbane, Queensland 4072, Australia

⁴Centre for Microscopy and Microanalysis, The University of Queensland, Brisbane, Queensland 4072, Australia

(Received 6 December 2019)

Strained HgTe thin films are typical three-dimensional topological insulator materials. Most works have focused on HgTe (100) films due to the topological properties resulting from uniaxial strain. In this study, strained HgTe (111) thin films are grown on GaAs (100) substrates with CdTe (111) buffer layers using molecular beam epitaxy (MBE). The optimal growth conditions for HgTe films are determined to be a growth temperature of 160°C and an Hg/Te flux ratio of 200. The strains of HgTe films with different thicknesses are investigated by high-resolution x-ray diffraction, including reciprocal space mapping measurements. The critical thickness of HgTe (111) film on CdTe/GaAs is estimated to be approximately 284 nm by Matthews' equations, consistent with the experimental results. Reflection high-energy electron diffraction and high-resolution transmission electron microscopy investigations indicate that high-quality HgTe films are obtained. This exploration of the MBE growth of HgTe (111) films provides valuable information for further studies of HgTe-based topological insulators.

PACS: 81.15.-z, 68.55.-a, 61.05.-a, 61.05.cp, 68.37.Og

DOI: 10.1088/0256-307X/37/3/038101

Owing to its zinc blende structure with reversed band structure, bulk HgTe exhibits semimetallic properties ($E_g = -0.3$ eV) and very strong spin-orbit coupling. When combined with the wide-bandgap semiconductor CdTe ($E_g = 1.6$ eV), the bandgap of $\text{Hg}_{1-x}\text{Cd}_x\text{Te}$ is tunable from -0.3 to 1.6 eV. $\text{Hg}_{1-x}\text{Cd}_x\text{Te}$ has become an important material for infrared photodetectors in the last half century because of its high detectivity, high quantum efficiency, and fast response time.^[1,2] In the past few decades, it was theoretically predicted and experimentally confirmed that the quantum spin Hall effect can be achieved in the HgTe/CdTe superlattice structure, generating a surge in research on topological insulator (TI) materials.^[3,4] In recent years, researchers have found that strained HgTe thin films are good three-dimensional TIs.^[5] Many novel physical properties are found in HgTe TIs, including ballistic edge states^[6,7] and topological surface states in bulk strained HgTe.^[5,8] Studies of HgTe are mainly carried out on its (100), (013), and (211) orientations.^[9–15] Only a few experimental studies have been reported on HgTe (111).^[16,17] Along the (111) orientation, HgTe shows a honeycomb lattice similar to graphene.^[18] The honeycomb structure of HgTe was predicted to exhibit a fractional Chern insulator or fractional quantum spin Hall state,^[19] and compressively strained (111) HgTe was predicted to be a TI.^[20,21] For the (110) and (100) orientations of HgTe, the four bands are linearly dispersed at the Γ point. However, two

of the four bands are quadratically dispersed along the HgTe (111) axis due to time-reversal and mirror symmetry.^[22,23] Furthermore, it is interesting to study high-quality strained HgTe (111) films.

In this work, the effect of film thickness on strain is studied theoretically and experimentally in HgTe (111) films. To improve the HgTe film quality, the properties of the HgTe–CdTe interface are investigated by reflection high-energy electron diffraction (RHEED) and high-resolution transmission electron microscopy (HRTEM). Finally, high-quality HgTe (111) films are obtained.

In our experiment, HgTe films were grown by molecular beam epitaxy (MBE, DCA 450, Finland). The substrate temperatures were measured by a pyrometer and a temperature monitor (kSA BandiT). The temperature monitor was calibrated at the GaAs deoxidizing temperature of 587°C to monitor the CdTe growth temperature. The pyrometer was calibrated at the indium melting temperature of 156°C to more accurately monitor the HgTe growth temperature. The CdTe (111) buffer layers and HgTe (111) films were grown on GaAs (100) substrates mounted on indium-free molybdenum blocks.

Before HgTe/CdTe growth, the GaAs (100) substrates were deoxidized at 596°C under As atmosphere. Through low-temperature nucleation at 250°C, a “seed” layer of CdTe with (111) orientation was deposited on the GaAs substrate. After nucleation, a standard CdTe layer was grown at 320°C with a

*Supported by the National Natural Science Foundation of China (Grant Nos. 11634009, 61874069, 1177041280 and 11574336), and Shanghai Science and Technology Foundation (Grant No.18JC1420401).

**Corresponding author. Email: ppchen@mail.sitp.ac.cn; wu_yan@mail.sitp.ac.cn

© 2020 Chinese Physical Society and IOP Publishing Ltd

growth rate of approximately $1.2 \mu\text{m/h}$. A CdTe buffer layer with a thickness of approximately $2.6 \mu\text{m}$ was deposited to release the strain between the CdTe layer and the GaAs substrate. The full width at half maximum (FWHM) of the CdTe (111) rocking curve was ~ 200 arcsec, and the rms roughness of the CdTe surface was determined by atomic force microscopy to be $\sim 0.79 \text{ nm}$. The high-quality CdTe buffer layer ensured the growth of a high-quality HgTe film. Finally, HgTe films were grown on the CdTe/GaAs composite substrates at $158\text{--}162^\circ\text{C}$ with a Hg:Te flux ratio of approximately 200 and a growth rate of approximately 0.02 ML/s .

To maintain the substrate temperature at 160°C , the substrate heater was controlled by the power mode because the thermocouple response speed is very slow at low temperature ($<200^\circ\text{C}$). On the indium-free molybdenum blocks, the CdTe/GaAs composite substrates transmit infrared radiation. Due to the infrared absorption characteristics of zero-gapped HgTe, after a thin HgTe layer was grown, the substrate temperature increased sharply. To keep the substrate temperature stable, the substrate power must be optimized. After growth, the HgTe thin films were annealed under Hg atmosphere at 130°C for 30 min. Finally, a 30-nm CdTe cap layer was deposited to protect the HgTe film.

The growth of the HgTe films was monitored by *in situ* RHEED, while the strain and crystalline quality

were then characterized using x-ray diffraction (XRD, Bruker D8 Discover). The structural characteristics of the thin films and their interfaces were investigated by TEM (FEI Tecnai F20 TEM). Cross-sectional TEM samples were prepared using a focused ion beam (FIB, FEI Scios).

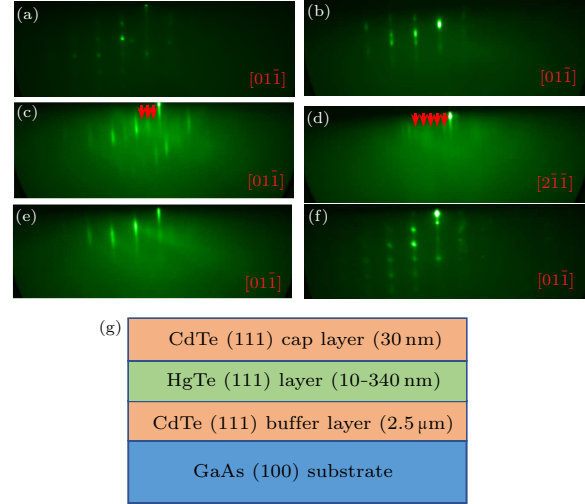


Fig. 1. (a) Polycrystalline and (b) twin-like RHEED patterns of HgTe with $[01\bar{1}]$ orientation. RHEED patterns of HgTe with (c) $[01\bar{1}]$ and (d) $[2\bar{1}\bar{1}]$ orientations showing sharp, single-crystalline lines with 4×6 reconstruction (red arrows). RHEED patterns of HgTe with $[01\bar{1}]$ orientation upon cooling down. (e) with and (f) without Hg atmosphere after growth. (g) diagram of HgTe films' layer structure.

Table 1. The HgTe films used in this work.

| Sample | CdTe buffer (μm) | HgTe (nm) | CdTe cap (nm) | Strain |
|--------|-------------------------------|-----------|---------------|-----------------|
| 1 | 2.6 | 66 | 30 | Strained |
| 2 | 2.6 | 128 | 30 | Strained |
| 3 | 2.6 | 223 | 30 | Strained |
| 4 | 2.6 | 340 | 30 | Strain-Released |
| 5 | 2.6 | 120 | 30 | Strained |
| 6 | 2.6 | 10 | 30 | Strained |

Figures 1(a) and 1(b) show the polycrystalline and twin-like RHEED patterns obtained during HgTe growth, respectively. It was reported that Hg deficiency leads to a polycrystalline RHEED pattern, whereas excess Hg flux results in twin-like RHEED patterns.^[16] When the Hg/Te flux ratio was maintained at ~ 200 , we found: (1) when the substrate temperature exceeded 163°C , the polycrystalline pattern appeared [Fig. 1(a)], in which peaks of miscellaneous phases emerge beside the standard RHEED pattern, and (2) when the substrate temperature was below 157°C , a twin-like pattern appeared [Fig. 1(b)], in which a twin-like double point replaces the standard RHEED pattern. It was reported that defects are easily induced in the early stage of HgTe (111) growth.^[16,17] Interfacial defects can be observed by RHEED when the temperature fluctuates by more than 3°C , these defects are especially obvious on the (111) surface since the twin boundaries are distributed in-plane.^[24] Figures 1(c) and 1(d) show that under proper growth conditions, the films exhibited crys-

tallinity along the $[01\bar{1}]$ and $[2\bar{1}\bar{1}]$ directions. The observed $c(4 \times 6)$ surface reconstructions indicate HgTe films with good crystalline quality.

Figures 1(e) and 1(f) show the RHEED patterns of HgTe after growth with and without Hg atmosphere, respectively. When the film was protected by Hg atmosphere, the sharp lines remained stable. Figure 1(g) shows the diagram of HgTe films' layer structure. However, when the Hg shutter was closed, the RHEED pattern indicated polycrystallinity (Hg deficiency), suggesting that HgTe is not stable at high temperature. Therefore, if the CdTe cap layer is not deposited after HgTe growth, the HgTe film should be cooled to 80°C under the protection of Hg atmosphere.

By optimizing the growth process, it was determined that the proper Hg/Te flux ratio for HgTe (111) film growth is ~ 200 at 160°C . A set of HgTe (111) samples with different thicknesses were grown under these conditions. Table 1 lists the thickness and properties of the HgTe samples in this work.

The HgTe film samples with thicknesses of 67 nm

(sample 1), 128 nm (sample 2), 223 nm (sample 3), and 340 nm (sample 4) were studied by high-resolution XRD (HRXRD). As shown in Fig. 2, a Pendellosung fringe period was observed in samples 1–3, which can be attributed to thickness interference in the high-quality films. When the film thickness exceeded the critical thickness, the stress relaxation process induced dislocations at the interface and in the HgTe layer. As a result, the interfacial oscillations disappeared in sample 4 with a HgTe thickness of 340 nm. These results agree with the theoretically calculated critical thickness of 284 nm. The HRXRD data (blue lines in Fig. 2) were obtained from 10 repeated integration scans. The simulated results (red lines in Fig. 2) were calculated by fitting software. The simulation model was for HgTe (111) films grown on CdTe (111) substrates, assuming that the 2.5- μm CdTe (111) buffer layer is fully strain-relaxed. The simulated results agree well with the experimental results for the samples 1–3. The average thickness of sample 2 was confirmed to be ~ 128 nm by HRTEM analysis of a cross-sectional FIB sample, confirming the accuracy of our calculation.

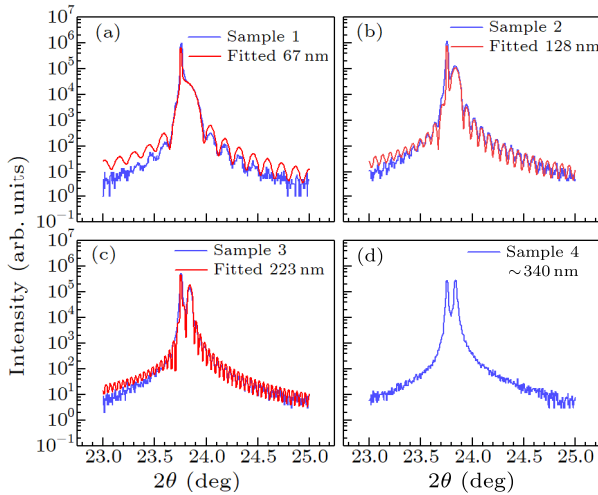


Fig. 2. HRXRD experimental data (blue lines) and simulated data obtained by fitting software (red lines) for the HgTe films with thicknesses: (a) 67 nm, (b) 128 nm, (c) 223 nm, and (d) 340 nm.

To study the elastic strain release properties of the HgTe (111) films on CdTe/GaAs (111) substrates, the critical thickness was calculated using Matthews' equations. The calculated critical thickness for an HgTe (111) film on a CdTe (111) substrate was approximately 284 nm. Figure 3(a) shows a plot of elastic strain versus the film thickness of HgTe with (111) orientation calculated using Matthews' equation.^[25] When the HgTe thickness is below 284 nm, the film is almost fully strained.

The theoretical epitaxial relationship between HgTe/CdTe (111) and the GaAs (100) substrate is shown in Fig. 3(b). For the out-of-plane orientation, the HgTe/CdTe [111] is parallel to GaAs [100]. For the in-plane orientation, HgTe/CdTe [01 $\bar{1}$] is parallel to GaAs [01 $\bar{1}$], and HgTe/CdTe [2 $\bar{1}\bar{1}$] is parallel to GaAs

[011]. The asymmetric (511) and (422) peaks were examined by reciprocal space mapping (RSM) to experimentally verify the epitaxial relationship. Figures 3(c) and 3(d) show the GaAs (511) and HgTe/CdTe (422) in-plane (Q_x) and out-plane (Q_z) peak positions, respectively, for sample 2. In Fig. 3(c), the azimuth value is 0° , the Q_x axis is parallel to GaAs [011] and HgTe/CdTe [2 $\bar{1}\bar{1}$] in real space, and the Q_z axis is parallel to GaAs [100] and HgTe/CdTe [111] in real space. The red-solid line in Fig. 3(c) is the experimental result for the relationship between the GaAs (511) and CdTe (422) peak positions, the red-dashed line is the theoretical result. The thickness of the CdTe buffer layer was ~ 2.5 μm to ensure that the strain was fully released. The difference between the theoretical and experimental results may arise from the transformation of the orientation of the CdTe (111) layer at the beginning of film growth on the GaAs (100) substrate. As shown in Fig. 3(d), we rotated the azimuth value by 90° to measure the GaAs (51 $\bar{1}$) peak, for which the Q_x axis is parallel to GaAs [01 $\bar{1}$] and HgTe/CdTe [01 $\bar{1}$] in real space, and the Q_z axis is parallel to GaAs [100] and HgTe/CdTe [111] in real space. Notably, the HgTe/CdTe (422) peak is not observed since the (422) peak rotational symmetry is approximately 60° rather than 90° .

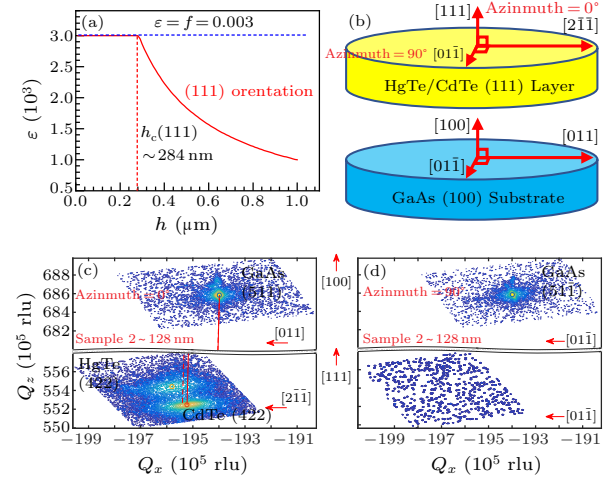


Fig. 3. (a) Elastic strain vs HgTe film thickness. The critical thickness calculated by Matthews' equations is 284 nm for the (111) orientation (red line). (b) Schematic diagrams of crystal orientation for a HgTe/CdTe (111) layer grown on a GaAs (100) substrate. (c) GaAs (511) and HgTe/CdTe (422) RSM results for sample 2 (thickness 128 nm). The red-solid line is the experimental result for the link between the GaAs (511) and CdTe (422) peak positions, the red-dashed line is the theoretical result. (d) GaAs (51 $\bar{1}$) RSM results for sample 2 (thickness 128 nm). The HgTe/CdTe (422) peak is not observed for the azimuth (plane angle) value of 90° .

To further analyze the relationship between strain and thickness, the asymmetric HgTe/CdTe (422) peaks were investigated using RSM. The RSM of the asymmetric peak provides in-plane and out-of-plane information for the study of relaxation. Figures 4 shows the RSM asymmetric (422) diffractions of samples 1–4. The peaks of the CdTe layer and thick HgTe

films are accompanied by detector streaks, because of their high intensities. In Fig. 4, Q_z and Q_x indicate the out-of-plane $[111]$ and in-plane $[2\bar{1}\bar{1}]$ orientations, respectively. The red-dashed lines in Fig. 4 indicate unstrained HgTe (422), while the red solid lines show the experimental results. As the thickness increases, the intensity of the HgTe (422) peak increases. As shown in Figs. 4(a), 4(b), and 4(c), the HgTe (422) peak positions are not located at the calculated unstrained lines, implying that the strain was not released in samples 1–3. In contrast, in Fig. 4(d), the HgTe (422) peak is located at the calculated unstrained line, indicating that the strain was released in sample 4 (thickness 340 nm). The HgTe (422) peak is broadened in Fig. 4(d) due to dislocations of stress relaxation. This is in agreement with the disappearance of thickness interference observed by HRXRD in Fig. 2(b). The calculated critical thickness for HgTe (111) on a CdTe (111) substrate was approximately 284 nm. Furthermore, the experimental and theoretical results are in good agreement.

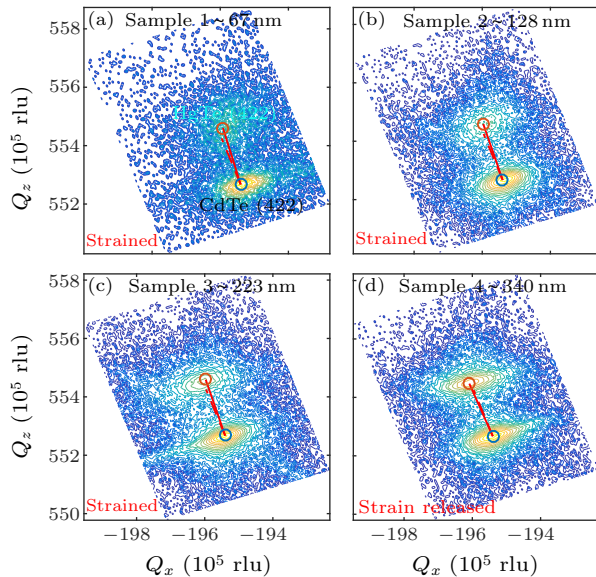


Fig. 4. RSM maps of HgTe around the asymmetric CdTe (422) peak for HgTe/CdTe(111) samples with different HgTe thickness: 67 nm (a), 128 nm (b), 223 nm (c), and 340 nm (d). The red lines indicate the unstrained material, and the intersections with the red-dotted lines indicate the unstrained HgTe (422) peak position.

A high-quality HgTe/CdTe interface is critical for obtaining high-quality HgTe quantum well films. Therefore, it is crucial to investigate the structural characteristics of the HgTe/CdTe interface. The interfaces of two HgTe/CdTe quantum well samples were investigated by HRTEM. At the beginning of HgTe growth in sample 5, when the substrate temperature was 3°C below the optimal temperature, the measured RHEED patterns indicate twin defects along the $[01\bar{1}]$ direction, which is parallel to the (111) surface. For sample 6, the RHEED patterns indicate twin-free films throughout the growth process.

Figures 5(a) and 5(b) show the typical HRTEM

images of the HgTe/CdTe interfaces in samples 5 and 6, respectively. In Fig. 5(a), a high density of defects (twin-like defects and dislocations) are observed in the HgTe/CdTe interfacial area, corresponding to the twin-like crystal double point observed in the RHEED pattern [Fig. 5(c)]. In contrast, Fig. 5(b) indicates that sample 6 has a perfect lattice-matched HgTe/CdTe interface without any observable defects, in agreement with the defect-free pattern in Fig. 5(c). Figure 5(d) shows the typical selected-area electron diffraction (SAED) patterns taken from the HgTe and CdTe layers along the $[01\bar{1}]$ zone axis. The miscellaneous free SAED patterns indicate that HgTe and CdTe layers were grown with high crystal quality.

The results demonstrate that during the growth of HgTe(111) on CdTe(111), twin-like defects are easily generated at the HgTe/CdTe interface. However, defect-free, high-quality HgTe/CdTe quantum wells can be obtained by carefully controlling and optimizing the MBE growth conditions of HgTe with monitoring by *in situ* RHEED.

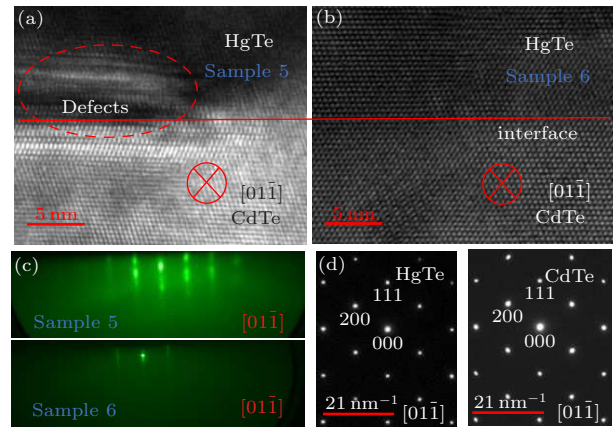


Fig. 5. HRTEM images of the HgTe/CdTe interface in (a) sample 5, in which defects are observed at the interface, and (b) sample 6, which has a defect-free interface. (c) RHEED patterns of sample 5 (twin-free pattern) and sample 6 (twin-free pattern) taken after 2 min of HgTe growth. (d) SAED patterns of the HgTe layer and CdTe buffer layer, indicating high crystalline quality in the bulk material.

In summary, we have successfully grown strained HgTe (111) films on CdTe (111)/GaAs (100) composite substrates. By optimizing the growth process, high-quality HgTe films are grown at a substrate temperature of 160°C and Hg/Te flux ratio of ~ 200 . The critical thickness of the HgTe film is calculated by Matthews' equations for (111)-orientated HgTe on CdTe. Detailed HRXRD and RSM results show that the critical thickness is ~ 284 nm for the (111) orientation. Twin-like defects were observed in the HgTe/CdTe interfacial area based on the RHEED patterns measured during HgTe growth. These defects were confirmed by HRTEM investigation. This exploration of the MBE growth of HgTe (111) films with high crystalline quality provides valuable information for further studies of HgTe-based TIs.

The Australian Microscopy & Microanalysis Research Facility is gratefully acknowledged for providing access to the facilities used in this work.

References

- [1] Lei W, Antoszewski J and Faraone L 2015 *Appl. Phys. Rev.* **2** 041303
- [2] Liu M, Wang C and Zhou L Q 2019 *Chin. Phys. B* **28** 037804
- [3] Bernevig B A, Hughes T L and Zhang S C 2006 *Science* **314** 1757
- [4] König M, Wiedmann S, Brüne C, Roth A, Buhmann H, Molenkamp L W, Qi X L and Zhang S C 2007 *Science* **318** 766
- [5] Brüne C, Liu C X, Novik E G, Hankiewicz E M, Buhmann H, Chen Y L, Qi X L, Shen Z X, Zhang S C and Molenkamp L W 2011 *Phys. Rev. Lett.* **106** 126803
- [6] Brüne C, Roth A, Novik E G, König M, Buhmann H, Hankiewicz E M, Hanke W, Sinova J and Molenkamp L W 2010 *Nat. Phys.* **6** 448
- [7] Nowack K C, Spanton E M, Baenninger M, König M, Kirtley J R, Kalisky B, Ames C, Leubner P, Brüne C, Buhmann H, Molenkamp L W, Goldhaber-Gordon D and Moler K A 2013 *Nat. Mater.* **12** 787
- [8] Savchenko M L, Kozlov D A, Vasilev N N, Kvon Z D, Mikhailov N N, Dvoretzky S A and Kolesnikov A V 2019 *Phys. Rev. B* **99** 195423
- [9] Ballingall J M, Leopold D J, Wroge M L, Peterman D J, Morris B J and Broerman J G 1986 *Appl. Phys. Lett.* **49** 871
- [10] Oehling S, Ehinger M, Spahn W, Waag A, Becker C R and Landwehr G 1996 *J. Appl. Phys.* **79** 748
- [11] Dvoretzky S, Mikhailov N, Sidorov Yu, Shvets V, Danilov S, Wittman B and Ganichev S 2010 *J. Electron. Mater.* **39** 918
- [12] Ballet P, Thomas C, Baudry X, Bouvier C, Crauste O, Meunier T, Badano G, Veillerot M, Barnes J P, Jouneau P H and Levy L P 2014 *J. Electron. Mater.* **43** 2955
- [13] Selvig E, Tonheim C R, Kongshaug K O, Skauli T, Lorentzen T and Haakenaasen R 2007 *J. Vac. Sci. Technol. B: Microelectron. Nanometer Struct. Process. Meas. Phenom.* **25** 1776
- [14] Thomas C, Baudry X, Barnes J P, Veillerot M, Jouneau P H, Pougetb S, Craustec O, Meunierc T, Lévy L P and Ballet P 2015 *J. Cryst. Growth* **425** 195
- [15] Leubner P, Lunczer L, Brüne C, Buhmann H and Molenkamp L W 2016 *Phys. Rev. Lett.* **117** 086403
- [16] Feldman R D, Nakahara S, Opila R L, Austin R F and Boone T 1989 *J. Cryst. Growth* **98** 581
- [17] Schaake H F and Koestner R J 1988 *J. Cryst. Growth* **86** 452
- [18] Yang X Y, Wang G Y, Zhao C X, Zhu Z, Dong L, Li A M, Lv Y Y, Yao S H, Chen Y B, Guan D D, Li Y Y, Zheng H, Qian D, Liu C H, Chen Y L and Jia J F 2018 *Chin. Phys. Lett.* **35** 026802
- [19] Beugeling W, Kalesaki E, Delerue C, Niquet Y M, Vanmaekelbergh D and Smith C M 2015 *Nat. Commun.* **6** 6316
- [20] Liang F, Kane C L and Mele E J 2007 *Phys. Rev. Lett.* **98** 106803
- [21] Zaheer S, Young S M, Cellucci D, Teo J C Y, Kane C L, Mele E J and Rappe A M 2013 *Phys. Rev. B* **87** 045202
- [22] Young S M, Zaheer S, Teo J C Y, Kane C L, Mele E J and Rappe A M 2012 *Phys. Rev. Lett.* **108** 140405
- [23] Dresselhaus G 1955 *Phys. Rev.* **100** 580
- [24] Selvig E, Tonheim C R, Lorentzen T, Kongshaug K O, Skauli T and Haakenaasen R 2008 *J. Electron. Mater.* **37** 1444
- [25] Matthews J W and Blakeslee A E 1974 *J. Cryst. Growth* **27** 118